Numerical Studies on the Effect of Delta-Shaped Obstacles

by Ekadewi Handoyo

Submission date: 26-Jun-2020 11:19PM (UTC+0700)
Submission ID: 1350065247
File name: 1-s2.0-S0038092X16001389-main_termuat_di_solar_energy.pdf (5.76M)
Word count: 8193
Character count: 38286

Available online at www.sciencedirect.com

ScienceDirect

Solar Energy 131 (2016) 47–60

SOLAR ENERGY

www.elsevier.com/locate/solener

Numerical studies on the effect of delta-shaped obstacles' spacing on the heat transfer and pressure drop in v-corrugated channel of solar air heater

Ekadewi A. Handoyo [a,*], Djatmiko Ichsani [b], Prabowo [b], Sutardi [b]

[a] Mechanical Engineering Dept, Petra Christian University, Surabaya, Indonesia
[b] Mechanical Engineering Dept, Institut Teknologi Sepuluh Nopember, Surabaya, Indonesia

Received 11 October 2015; received in revised form 9 February 2016; accepted 16 February 2016

Communicated by: Associate Editor Bibek Bandyopadhyay

Abstract

Solar air heater (SAH) is simple in construction compared to solar water heater. Yet, it is very useful for drying or space heating. Unfortunately, the convective heat transfer between the absorber plate and the air inside the solar air heater is rather low. Some researchers reported that obstacles are able to enhance the heat transfer in a flat plate solar air collector and others found that a v-corrugated absorber plate gives better heat transfer than a flat plate. Only a few research combines these two in a SAH. This paper will describe the combination from other point of view, i.e. the spacing between obstacles. Its spacing possibly will effect the heat transfer and pressure drop of the air flowing across the channel.

The first step in numerical study is generating mesh or grid of the air flow inside a v-corrugated channel which was blocked by some delta-shaped obstacles. The mesh was designed three-dimension and not uniform. The mesh are made finer for area near obstacles and walls both for upper and bottom, and then gradually coarser. Grid independency is the next step to be conducted. When the mesh is already independent, the numerical study begins. To validate the numerical model, an indoor experiment was conducted. Turbulent model used was Shear Stress Transport K-ω (SSTK-ω) standard. Having a valid numerical model, the spacing between obstacles was studied numerically. Ratio spacing to height, S/H of obstacles investigated were 0.5; 1; 1.5; and 2.

From numerical studies in a v-corrugated duct, it is found that backflow between obstacles and high velocity in the gap between obstacles and absorber plate causes the flow became more turbulent and enhanced the convection heat transfer between the air and the absorber plate. Obstacles placed in a small spacing will increase Nusselt number (convection heat transfer) and friction factor (pressure drop). The Nusselt number enhanced from 27.2 when no obstacle used to 94.2 when obstacles inserted with $S/H = 0.5$. The Nusselt enhanced 3.46 times. The friction factor will increase from 0.0316 at no obstacle to 0.628 at ratio $S/H = 0.5$. The friction factor increased 19.9 times. Efficiency, Nusselt number, and friction factor are decreasing as ratio S/H is increasing. When ratio S/H used is 1 instead of 0.5, Nusselt number enhancement decreased only 1.13%, but friction factor decreased 15.1%. So, sacrificing a small amount of Nusselt number but reducing a significant friction factor is advantageous. The optimal spacing ratio S/H of delta-shaped obstacles inserted in a v-corrugated SAH is one. In other words, the optimal spacing of obstacle equals to its height.

Keywords: Delta-shaped obstacle; v-corrugated channel; Solar air heater; Numerical study

* Corresponding author.
E-mail address: ekadewi@petra.ac.id (E.A. Handoyo).

http://dx.doi.org/10.1016/j.solener.2016.02.031
0038-092X/

Nomenclature

W	wide of the obstacle (mm)	T_{abs}	absorber temperature (K)
H	height of the obstacle (mm)	D_h	hydraulic diameter (m)
S	spacing between the obstacles (mm)	Nu_D	Nusselt number
x, y, z	coordinates	h	convection heat transfer coefficient (W/m^2 K)
Re	Reynolds number	f	friction factor
C_p	specific heat of air (J/kg K)	ϑ	air kinematic viscosity (m^2/s)
$\dot{m}_f$	mass flow rate of the fluid–air (kg/s)	ρ	air density (kg/m^3)
$\dot{Q}_u$	useful heat transfer rate (W)	k	thermal conductivity (W/m K)
I	radiation intensity (W/m^2)	α	air thermal diffusion coefficient (m^2/s)
A_c	collector aperture area (m^2)	η	thermal efficiency of SAH
T_o	collector outlet temperature (K)		
T_i	collector air inlet temperature (K)		

1. Introduction

Solar energy can be converted into thermal energy in a solar collector. Solar collector basically is device used to trap solar energy to heat a plate and transfer the heat to a fluid flowing under or above the plate. When sun light falls onto a plate, solar radiation reaches the plate at lower wavelength and heat it up. Then, the heat is carried away by either water or air that flows under or above the plate. Solar collector used to heat up air is called solar air heater (SAH) and solar water heater for water. Generally, the solar air heater is less efficient than the solar water heater, because air has less thermal capacity and less convection heat transfer coefficient. Yet, air is much lighter and less corrosive than water. The other benefit is that heated air can be used for moderate-temperature drying, such as harvested grains or fish. Since the solar air heater has less convective heat transfer coefficient than solar water heater, some researchers tried to increase this convective heat transfer coefficient.

A popular type of solar air heater is the flat plate SAH, which has a cover glass on the top, insulation on the sides and bottom to prevent heat transferred to the surrounding, a flat absorber plate that makes a passage for the air flowing with sides and bottom plate. Usually, the passage or channel has a rectangular cross-section. The absorber plate will transfer the heat to the air via convection. Unfortunately, the convection coefficient is very low. To increase the convection coefficient from the absorber plate, a v-corrugated plate is used instead of a flat plate. Tao et al. (2007) stated that a solar air heater with a v-grooved absorber plate could reach efficiency 18% higher than the flat plate on the same operation condition and dimension or configuration. Karim dan and Hawlader (2006) found that a solar collector with a v-absorber plate gave the highest efficiency and the flat plate gave the least. The results showed that the v-corrugated collector is 10–15% and 5–11% more efficient in single pass and double pass modes, respectively, compared to the flat plate collectors. Choudhury dan and Garg (1991) made a detailed analysis of corrugated and flat plate solar air heaters of five different configurations. For the same length, mass flow rate, and air velocity, it was found out that the corrugated and double cover glass collector gave the highest efficiency. According to Naphon (2007) the corrugated surfaces give a significant effect on the enhancement of heat transfer and pressure drop. The Nusselt number of flow in a v-corrugated channel can be 3.2–5.0 times higher than in a plane surfaces while the pressure drop 1.96 times higher than on the corresponding plane surface. Islamoglu dan and Parmaksizoglu (2003) reported that the corrugated channel gave the higher Nusselt number than the straight channel and the higher channel height gave higher Nusselt number for the flow with the same Reynolds number.

Besides changing the cross section area of the channel, some also give effort to increase turbulence inside the channel with fins or obstacles. The result of experimental study done by Promvonge (2010) in turbulent flow regime (Reynolds number of 5000–25,000) showed that multiple 60° V-baffle turbulator fitted on a channel provides the drastic increase in Nusselt number, friction factor, and the thermal enhancement factor values over the smooth wall channel. Promvonge found that Nusselt number was five times higher and friction factor was 30 times than without baffle at Reynolds number = 10000, $e/H = 0.3$, and $P_R = 1$. Kurtbas dan and Turgut (2006) investigated the effect of fins located on the absorber surface in free and fixed manners. They used two kinds of rectangular fins which dimension is different but total area is the same. The first type fin (I) has dimension 810 × 60 mm and the second (II) type 200 × 60 mm. To have the same total area, there are 8 fins and 32 fins for the first and second, respectively. The fins type II, both free and fixed, were more effective than type I and flat-plate collector. The fixed fin collector was more effective than free fin collector. Kurtbas and Turgut reported that the maximum Instantaneous efficiency of SAH was 0.78 at air mass flow rate 0.08 kg/s when the fix fins type II were used. While the efficiency of flat plate

SAH was only 0.42. So, its efficiency increased 1.86 times. Romdhane (2007) created turbulence in the air channel using obstacles or baffles. The efficiency of collector and the air temperature was found increasing with the use of baffles. Baffles should be used to guide the flow toward the absorber plate. Romdhane reported that the efficiency reached 80% for the best type of baffle (chicane) for an air flow rate of 50 $m^3/h/m^2$. This efficiency was about 1.6 times efficiency without baffle. Ho et al. (2011) inserted fins attached by baffles and external recycling to a solar air heater. The experiment and theoretical investigations gave result that heat transfer was improved by employing baffled double-pass with external recycling and fin attached over and under absorber plate. According to Ho et al., the highest collector efficiency was 61% in a double-pass flat-plate SAH with recycle when radiation intensity was 1100 W/m^2, 24 fins attached, and mass flow rate was 0.02 kg/s. It was about 1.35 times its efficiency when there is no recycle. Abene et al. (2004) used obstacles on the flat plate of a solar air collector for drying grape. The obstacles ensure a good air flow over the absorber plate, create the turbulence and reduce the dead zones in the collector. The highest efficiency got was 70% when the air flow rate was 50 $m^3/h/m^2$. It was about 1.9 times its efficiency when no obstacle used. The air pressure drop increased about twice with obstacles. Esen (2008) used a double-flow solar air heater to investigate three different type obstacles placed on absorber plates compare with the flat plate. The collector has three absorber plates to make three passages for the air flowing through. From the research done, it was found that all collectors with obstacles gave higher efficiency than the flat plate and type III obstacles with flow in middle passage gave the highest efficiency, i.e. 52.9%, for air flow 0.02 kg/s. It was about 1.13 times higher than its efficiency with no obstacle. Ozgen et al. (2009) used aluminum cans as obstacles installed over and under absorber plate. They found that the SAH using double flow passage (over and under absorber plate) gave higher efficiency than just one flow passage (either over or under absorber plate). They also found that SAH with staggered cans (type I) had the highest efficiency compared to aligned cans (type II) and flat plat (type III). The efficiency of SAH type I was 0.73 at air flow rate 0.05 kg/s and it was about 1.4 times of type III. Akpinar dan and Koçyiğit (2010) had experimental investigation on solar air heater with several obstacles (Types I–III) and without obstacles. The optimal value of efficiency was obtained for the solar air heater with Type II obstacles on absorber plate in flow channel duct for all operating conditions and the collector with obstacles appears significantly better than that without obstacles. The efficiency of Type II was 0.6 at air flow rate 0.0052 kg/s and it was about twice of SAH without obstacle. Bekele et al. (2011) investigated experimentally the effect of delta shaped obstacles mounted on the absorber surface of an air heater duct. They found that the obstacle mounted duct enhances the heat transfer to the air. The heat transfer got higher if the obstacle height was taller and its longitudinal pitch was smaller. Nusselt number increased 3.5 times when obstacles inserted with ratio of longitudinal pitch $P_l/e = 3/2$ and height $e/H = 0.75$ at Reynolds number was 10,000. While its friction factor increased 4.7 times than without obstacle. SAH can be modeled through least-squares support vector machines (LS-SVM) method as done by Esen et al. (2009a). The predicted results from LS-SVM model had been compared to experimental results. LS-SVM could be used to predict the efficiency of SAH. They ashowed that efficiency of type I SAH was the highest. Esen et al. (2009b) also proposed Artificial Neural Network and Wavelet Neural Network (ANN and WNN) to predict the efficiency of SAH. They succeeded to show that the method could predict the SAH efficiency.

The combine of those two findings, i.e. obstacles and v-corrugated absorber plate are able to improve SAH are important to be studied. Handoyo et al. (2014) reported that the obstacles are able to enhance heat transfer in a v-corrugated SAH but increase the air pressure drop. To reduce the air pressure drop, the obstacles were bent vertically. The optimal bending angle is 30°. The SAH's efficiency was 5.3% lower when the obstacles bent 30° instead of straight (0°), but the pressure drop was 17.2% lower.

According to Incropera dan and DeWitt (2002), in forced convection heat transfer, there are two quantities that are important to be determined. One is friction coefficient, C_f, and the other is Nusselt number, Nu. Friction coefficient, C_f is used to calculate the shear stress at the wall and then to calculate pressure drop. While Nusselt number, Nu is used to calculate convection heat transfer rate. The relation that correlate them is known as Reynolds Analogy: $C_{f,x}\frac{Re_L}{2} = Nu_x Pr^{-1/3}$

When Nusselt number increases, then friction coefficient will increase, too. In a SAH, it is expected that convection heat transfer increases but pressure drop does not. So, many research were conducted to look for increasing in heat transfer at low pressure drop.

The spacing between obstacles mounted on absorber plate can be varied. A different spacing will give different air pressure drop as the air flows across the collector. Obstacles increase the air pressure drop. When the spacing is large, the obstacles used is less and the air pressure drop will be reduced. What about the heat transfer from the absorber plate to the flowing air? How will the spacing between obstacles effect the heat transfer? To the knowledge of the authors, there is no research investigating the effect of delta-shaped obstacles' spacing on a v-corrugated SAH performance yet.

This paper describes the result of the numerical studies of obstacles' spacing inserted in a v-corrugated channel of a SAH. The heat transfer from the v-corrugated absorber plate and the air pressure drop flowing the v-corrugated channel is to be discussed. The obstacles are delta-shaped and installed on bottom plate of the channel.

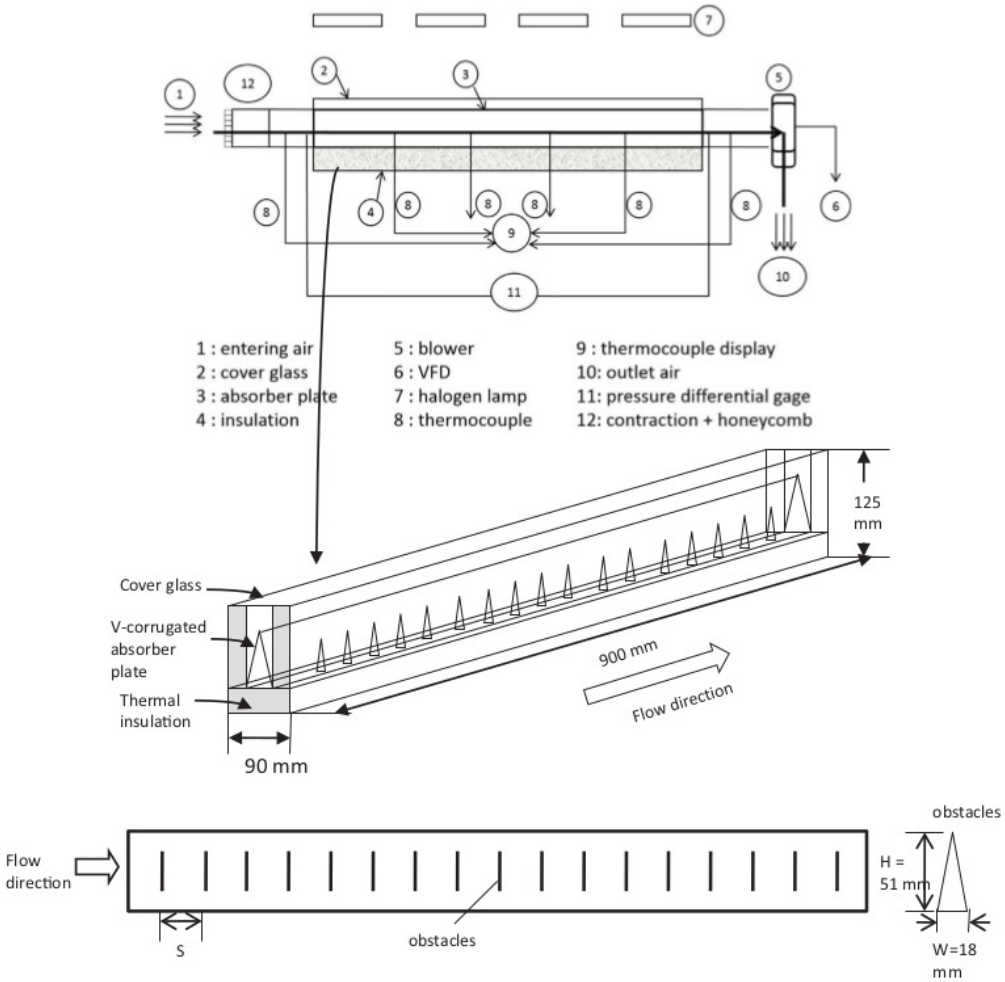

(a) Schematic of the solar collector model

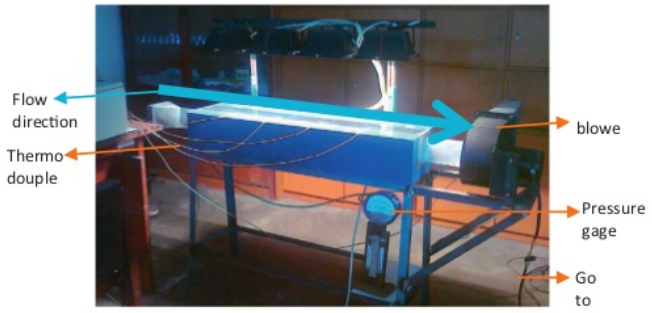

(b) Photograph of experimental set-up.

Fig. 1. The SAH model used in experiment.

2. Experimental set-up

The studies began with choosing a solar collector model to be studied. The study will be conducted numerically. Thus, a validation is required to prove that the result is true. The validation is accomplished via experiment. An indoor experiment model was constructed to validate numerical result. It is a model of SAH using v-corrugated absorber plate. Its schematic view and photograph are shown in Fig. 1(a) and (b), respectively. The experiment

was conducted in a laboratory of Mechanical Engineering Dept of Petra Christian University, Surabaya, Indonesia.

The collector model's dimension was 900 mm long, 90 mm width, and 125 mm height. A single 3-mm transparent-tempered glass was used as the collector cover. The v-corrugated absorber plate was made of 0.8-mm-thick aluminum and painted black. The apex angle of the v-corrugated plate was 20°. The v-corrugated channel's cross section was 30 mm width and 85 mm height. To prevent heat loss, the left and right walls of collector are insulated with a 25-mm Styrofoam each and a 35-mm Styrofoam for the bottom. The delta-shaped obstacles were made congruent to the channel i.e. triangular and its dimension was 18 mm wide, 51 mm height.

The experiment was conducted indoor to maintain the radiation intensity, wind's velocity and temperature. So, a bias result caused by different outdoor condition could be avoided. The sunlight is replaced with four 500-W halogen lamps. The radiation intensity received on the collector was measured using a pyranometer (Kipp & Zonen, type SP Lite2) placed on top of the cover glass. To ensure the homogenous intensity and to generate a certain absorber plate's temperature, these lamps were equipped with adjustable turner individually. The surrounding air condition was controlled by an air conditioner installed in the room. Its temperature, humidity, and wind velocity are well controlled. The collector was equipped with T-type thermocouple which accuracy is 0.1 °C for measuring the air temperature at inlet and outlet of the collector, temperature of the absorber plate (at four different locations), and ambient temperature. The pressure drop between inlet and outlet of the flowing air across the collector is also measured with a Magnehelic differential pressure gage which accuracy is ±2 Pa. A centrifugal blower (1000 m^3/h, 580 Pa, 0.2 kW, 380 V input) was used to induce the air flowing through the collector. The air flow was adjusted by means of a variable-frequency drive (VFD) to be 5.0 m/s (or Reynolds number = 10,000). The air flow is measured using digital anemometer which accuracy is ±0.1 m/s. All of the measurement equipments such as pressure gages and thermocouples are installed according to ASHRAE requirement (ASHRAE, 1986).

3. Numerical set up

The discussion in this paper is on the heat transferred to the flowing air and its pressure drop, then the domain of numerical study is focused on the air flow inside the v-corrugated channel. The apex angle of the v-corrugated channel is 20°. Its dimension was 900 mm long, 30 mm width, and 85 mm height. The delta-shaped obstacles were made congruent to the channel i.e. triangular and its dimension was 18 mm wide, 51 mm height. The obstacles were installed in one line only, because there is no much space in the channel. Thus, the spacing to be discussed is also called longitudinal pitch. To specify the obstacles' spacing, a ratio of spacing to height S/H is used. In this study, the ratio S/H used were ø, 1, 1 ø, and 2.

The numerical model for this problem was developed under some assumptions, i.e. as steady three-dimensional turbulent, incompressible flow and constant fluid properties. The space of obstacles was taken equal to height of obstacles, thus ratio is 1. Then, there are 17 obstacles used in this flow. Body force and viscous dissipation are ignored and it was assumed no radiation heat transfer. With these assumptions, (Incropera dan and DeWitt, 2002) give the related governing equations as follow:

$$\frac{\partial u}{\partial x}+\frac{\partial v}{\partial y}+\frac{\partial w}{\partial z}=0 \tag{1}$$

$$u\frac{\partial u}{\partial x}+v\frac{\partial u}{\partial y}+w\frac{\partial u}{\partial z}=-\frac{1}{\rho}\frac{\partial P}{\partial x}+\vartheta\left(\frac{\partial^2 u}{\partial x^2}+\frac{\partial^2 u}{\partial y^2}+\frac{\partial^2 u}{\partial z^2}\right) \tag{2}$$

$$u\frac{\partial v}{\partial x}+v\frac{\partial v}{\partial y}+w\frac{\partial v}{\partial z}=-\frac{1}{\rho}\frac{\partial P}{\partial y}+\vartheta\left(\frac{\partial^2 v}{\partial x^2}+\frac{\partial^2 v}{\partial y^2}+\frac{\partial^2 v}{\partial z^2}\right) \tag{3}$$

$$u\frac{\partial w}{\partial x}+v\frac{\partial w}{\partial y}+w\frac{\partial w}{\partial z}=-\frac{1}{\rho}\frac{\partial P}{\partial z}+\vartheta\left(\frac{\partial^2 w}{\partial x^2}+\frac{\partial^2 w}{\partial y^2}+\frac{\partial^2 w}{\partial z^2}\right) \tag{4}$$

$$u\frac{\partial T}{\partial x}+v\frac{\partial T}{\partial y}+w\frac{\partial T}{\partial z}=\alpha\left(\frac{\partial^2 T}{\partial x^2}+\frac{\partial^2 T}{\partial y^2}+\frac{\partial^2 T}{\partial z^2}\right) \tag{5}$$

In the above equations, ρ is the density of the air, p is the pressure, ϑ is the kinematic viscosity, α is the thermal diffusivity, and T is the temperature of the fluid. The boundary conditions of this problem were:

At the inlet: $u = 5.0$ m/s, $v = w = 0$, $T = 297.46$ K
At the upper wall which is the absorber plate: $u = v = w = 0$
At the bottom wall: $u = v = w = 0$
On the 17 obstacles: $u = v = w = 0$

Inlet Reynolds number was calculated with : Re

$$=\frac{uD_h}{\vartheta} \tag{6}$$

In Eq. (6), D_h is hydraulic diameter and calculated with:

$$D_h=\frac{4A}{P} \tag{7}$$

The area, A, in Eq. (7) is the channel cross section area, and P, is its perimeter.

The governing equations above with the boundary conditions were solved using a commercial CFD package, FLUENT 6.3.26 (FLUENT, 2003). The grids of the domain were generated using Gambit 2.4.6. The domain and meshing used in this numerical study were shown in Fig. 2. Since the geometry is a triangular channel, the numerical study should be conducted in three dimensions and all of the meshes were designed to have quality less than 0.7.

After having a good mesh, the next step is doing grid independency. The grid or mesh is made smaller to get more accurate and detailed result. But, when the mesh is

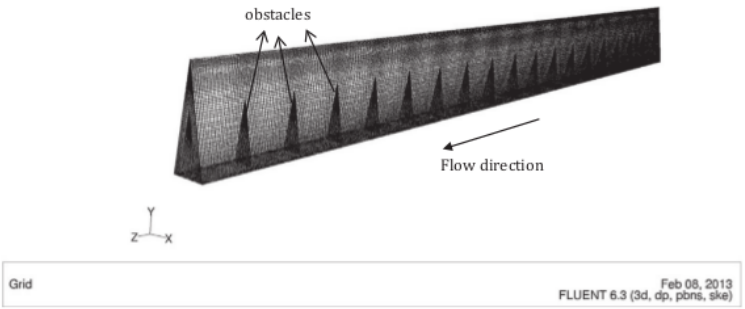

Fig. 2. The grid used in numerical studies.

too small, calculation which is done by iteration needs a very long time and might end up with diverge result. Therefore, in this study the mesh or grids were designed not uniform. The finer mesh are used for area near walls both for upper and bottom walls and then gradually the mesh are made coarser as shown in Fig. 2. When there are obstacles in the flow, the mesh are designed to be finer not only near the walls but also around the obstacles in Fig. 2. There are four meshes designs to be checked for independency as shown in Fig. 3(a)–(d). The number of cells, faces, and nodes used in each design are shown in Table 1.

To check the grid independency, the result from numerical study will be compared to experiment result. The same boundary conditions and setting are used in each numerical study of the four grids design as in Fig. 3. The boundary conditions are: inlet air velocity = 5.0 m/s and outflow was employed for the outlet; inlet air temperature = 297.46 K; and absorber plate temperature as obtained during experiments = 320 K. The settings in software used are: three dimension, double precision. Shear Stress Transport K-ω (SSTK-ω) standard turbulent model is chosen to simulate the flow. Zhang and Liu conducted numerical simulation of the flow inside a diffusing S-duct inlet. Full three-dimensional Navier–Stokes equations are solved and SST turbulence model is employed. Numerical results, include surface static pressure, total pressure recovery at exit, are compared with experiment. A fairly good agreement is apparent (Zhangdan and Liu, 2009). Other researcher, Kirkgoz et al. reported that numerical modeling using K-ω and SSTK-ω used on the cylinder surface gave reasonably success result (Kirkgoz et al., 2009). The SIMPLEC algorithm was employed to deal with the problem of velocity and pressure coupling. Second-order upwind scheme were used to discretize the main governing equations. Material of the absorber, bottom plate and the obstacles is aluminum. Fluid was air with inlet pressure 1 atm and its properties, such as density, viscosity, thermal conductivity were function of temperature.

Numerical studies were conducted for each of the four Mesh: A, B, C, and D. Fig. 4 shows global properties resulted from the numerical studies. They were the inlet and outlet temperature of air flowing through the channel and its pressure drop. Only Mesh B could not converge and the residual could not meet the criteria. So, there was no result of Mesh B in Fig. 4.

The experiment result which will be discussed in Section 4 gives pressure drop as much as 397.7 Pa, air temperature outlet 40.7 °C when the air inlet velocity is 5.0 m/s and inlet air temperature 24.5 °C.

Fig. 4 shows that numerical study with Mesh C and D give better result of air temperature compare to experiment than Mesh A, but Mesh D gives too high pressure drop result. Numerical studies using Mesh C give the most closely result to experiments. Thus, Mesh C was chosen for the numerical studies.

Using Mesh C pattern, some numerical studies were conducted to know the effect of obstacles' spacing. The ratio of spacing to height, S/H, studied numerically were ø, 1, 1 ø, and 2. The Mesh used in this study are in Fig. 5a–d. When the ratio S/H is bigger, then the number of obstacle is less. Number of obstacles are 8, 11, 17, and 35 for ratio $S/H = 2$, 1 ø, 1, and ø, respectively.

To give more comprehensive result, numerical study was also conducted for air flow in a v-corrugated channel without obstacle. The domain and mesh used is shown in Fig. 6.

4. Results and discussion

Since the experiment is conducted to validate the numerical result, then it is not necessary to conduct experiments for all ratio S/H. The ratio S/H used in experiment equals to 1. Thus, there are 17 obstacles inserted and the percentage of air flow blockage in the channel is 36%. The experiment followed the numerical setting. The experiments were conducted at certain inlet air velocity and certain radiation intensity or absorber temperature. A VFD was used to get an inlet air velocity equals to 5.0 m/s. An adjustable turner was used to adjust the radiation intensity that make the absorber's temperature as high as 320 K or 47 °C.

When the numerical result is close to the experimental result, then the numerical result is valid. Table 2 shows the comparison between numerical and experimental results at 5.0-m/s-inlet air velocity and 320 K absorber temperature. The air temperature difference and pressure drop

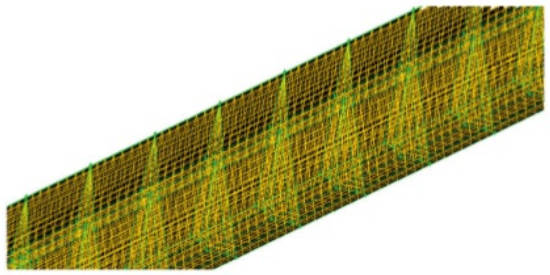

(a) Mesh A (most coarse)

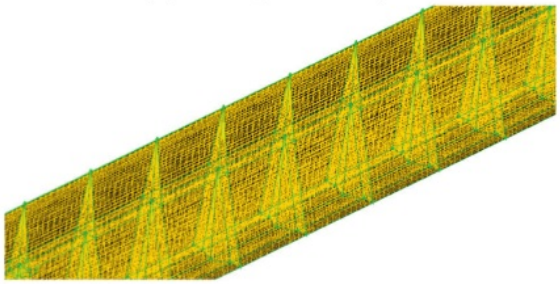

(b) Mesh B (slight coarse)

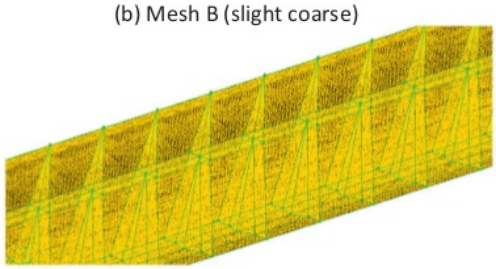

(c) Mesh C (slight fine)

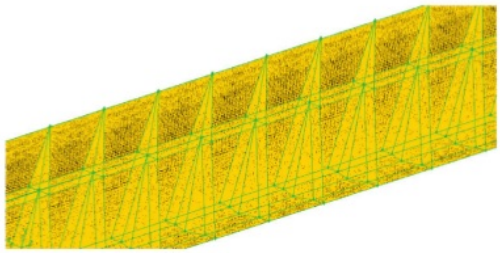

(d) Mesh D (most fine)

Fig. 3. Mesh design checked for independency.

Table 1
Number of cells, faces, and nodes of the four mesh design.

	Mesh A	Mesh B	Mesh C	Mesh D
Cell	55,296	338,688	1,092,000	1,980,000
Face	173,936	1,043,224	3,335,300	6,026,900
Node	63,172	365,480	1,150,798	2,066,248

of numeric is very close to experiment. Thus, the numerical study using several setting discussed above is acceptable and valid.

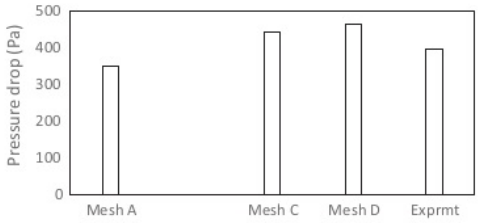

(a) The air pressure drop from numerical studies compared to experiment

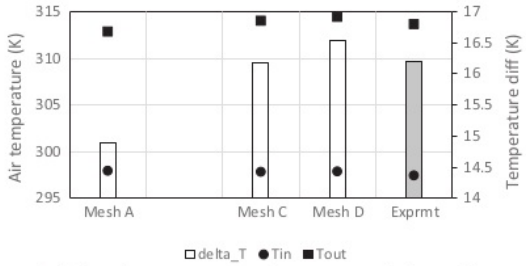

(b) The air temperature from numerical studies compared to experiment

Fig. 4. The numerical studies of Mesh A, C, and D compared to the result of experiment for $S/H = 1$.

To ensure that the model used in numerical study is valid, a comparison between Nusselt number from numerical result and Gnielinski equation for triangular channel without obstacle or smooth duct was conducted. According to Incropera dan and DeWitt (2002), Gnielinski gives more accurate relation to calculate Nusselt number at lower Reynolds number than Dittus–Boelter equation. The relation of Nusselt number is in Eq. (8):

$$Nu_D = \frac{(f/8)(Re_D - 1000)Pr}{1 + 12.7(f/8)^{1/2}(Pr^{2/3} - 1)} \tag{8}$$

The friction factor in Eq. (8), f, is obtained from Moody diagram. The comparison in Fig. 7 shows that numerical simulation gives pretty accurate results.

Having a valid grids, setting, and viscous model, the numerical study was continued to investigate the spacing effect of obstacles on the bottom plate of air duct. Diagrams of velocity vector of air flow around the obstacles inserted at ratio S/H equals to 2, 1 ø, 1, and ø are shown in Fig. 8(a)–(d), respectively. All of the velocity vectors were taken at height $y = 10$ mm from the bottom plate. When the ratio $S/H = 2$, the spacing between obstacles = 100 mm. For ratio $S/H = 1$ ø, the spacing = 75 mm, and for ratio $S/H =$ ø, the spacing = 25 mm.

Fig. 8(a)–(d) shows how the air flow encounters separation when flow through obstacles. The obstacles cause backflow between two consecutive obstacles in downstream. There are more backflows when the obstacles' spacing are closer and they cause a higher pressure drop. The air velocity looks higher near absorber plate when

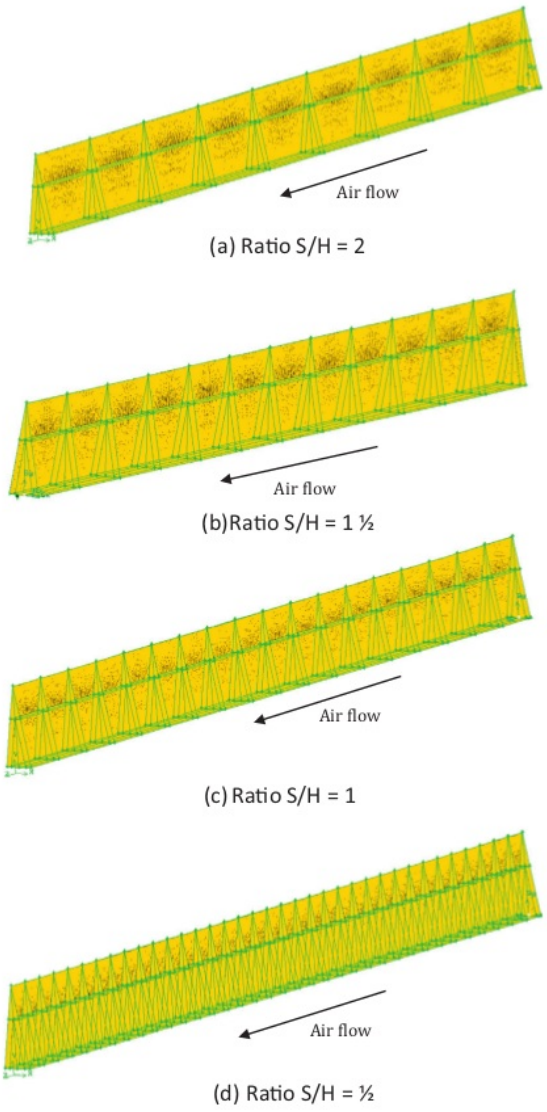

Fig. 5. The Mesh used for numerical studies of each spacing to height ratio, S/H.

Table 2
Comparison between numerical and experimental results.

	Numeric	Experiment
T_{in} (K)	297.9	297.5
T_{out} (K)	314.4	313.7
delta T (K)	16.5	16.2
delta P (Pa)	462.3	450.3

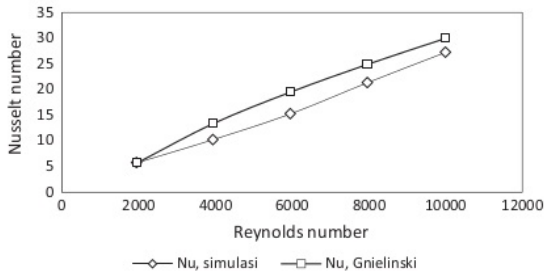

Fig. 7. Comparison of Nusselt number for smooth duct (no obstacle) from numerical study and Gnielinski equation.

there is backflow or swirl in the flow. This high air velocity makes flow become more turbulent and more heat transferred from the absorber plate to the air. This convection heat transfer to the air makes outlet air temperature higher. Thus, the closer the obstacles' spacing makes the higher pressure drop and higher convection heat transfer from the absorber plate to the air flow.

When the spacing between obstacles is twice its height (ratio $S/H = 2$), small amount of air flow is blocked by obstacles and causes backflow behind the obstacles. The backflow caused by separation gradually diminish between two obstacles in downstream as shown in Fig. 8(a). Since the air is blocked, most of air is forced to flow in the gap between obstacles and absorber plate. It is shown by longer and higher vector of velocity in the gap. More air is heated by absorber plate. Furthermore, higher velocity increases Reynolds number and make the flow more turbulent. More turbulent flow gives higher Nusselt number and definitely increase the convection heat transfer. Thus, obstacles makes outlet air temperature higher than without any

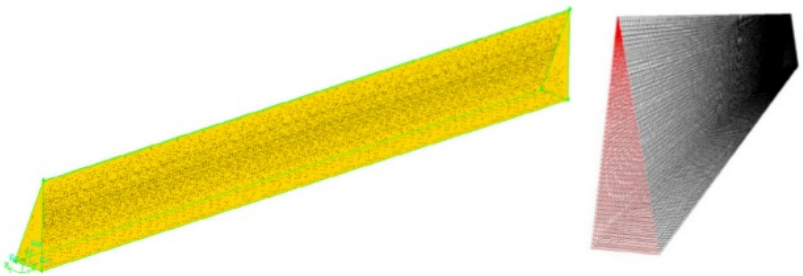

Fig. 6. The Mesh used for numerical studies of air flow without obstacle.

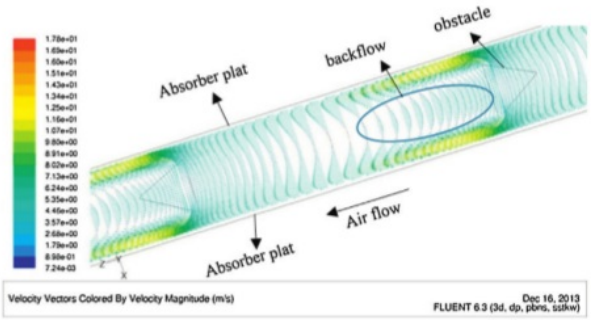

(a) Velocity vector of air flow around *obstacle* with ratio S/H = 2

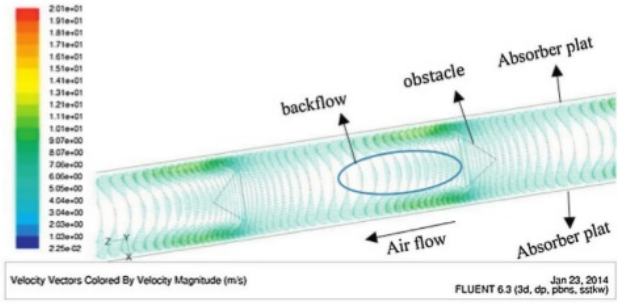

(b) Velocity vector of air flow around *obstacle* with ratio S/H = 1 ½

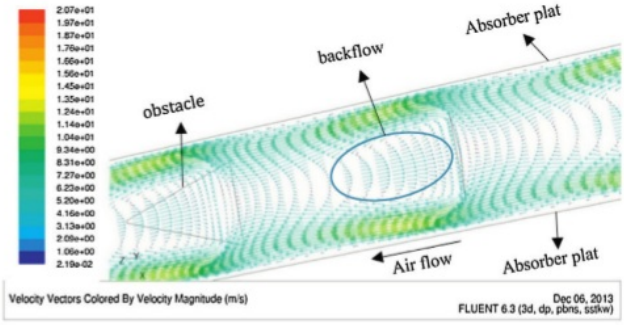

(c) Velocity vector of air flow around *obstacle* with ratio S/H = 1

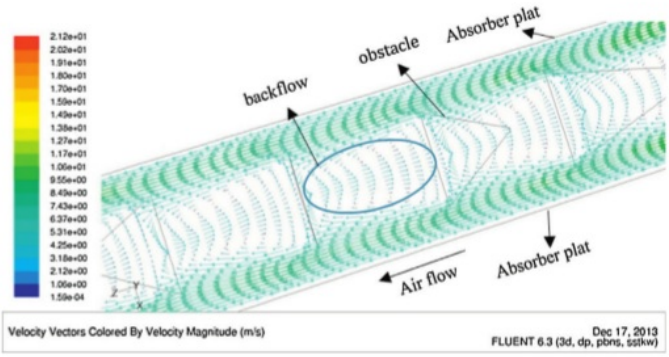

(d) Velocity vector of air flow around obstacle with ratio S/H = ½

Fig. 8. Velocity vector of air flow around obstacle with some ratio S/H.

(Handoyo et al., 2014). Flow in spacing between obstacles experiences backflow after hitting obstacles and then it reattaches quickly when the ratio $S/H = 2$. When the ratio S/H or spacing between obstacles is smaller, as shown in Fig. 8(b)–(d), backflow is more dominant than reattached flow in area between the obstacles. When backflow occurs, more air will flow in the gap and contact with absorber plate which is the heat source. It is the reason that smaller obstacles' spacing makes higher air outlet temperature and higher SAH's efficiency. The backflow in space between obstacles contributes pressure drop in the flow. More backflow causes higher pressure drop in air acrossed the v-corrugated absorber plate SAH.

Numerical studies also provide some global properties of the flow, such as the air inlet and outlet temperature, and pressure drop. These data were used to acquire the efficiency and friction factor of the air flow in a v-corrugated SAH with delta-shaped obstacles. The efficiency and friction factor are calculated using Eqs. (9) and (10) according to Duffie dan and Beckman (1991).

$$\eta = \frac{q_u}{A_c I} = \frac{\dot{m}_f c_p (T_{fo} - T_{fi})}{A_c I} \tag{9}$$

$$f = \frac{\Delta P}{\frac{L}{D_h}\rho\frac{v^2}{2}} \tag{10}$$

Comparison of efficiency and friction factor for some ratio S/H from numerical studies is shown in Fig. 9. Ratio $S/H = 0$ in Fig. 9 means no obstacle in the air flow. Obstacles arranged with ratio $S/H = ø$ gives the highest air efficiency, i.e. 68% and also highest friction factor, i.e. 0.628 for air flowing in a v-corrugated duct, as shown in Fig. 9. For comparison, efficiency when no obstacle is only 49% and friction factor is only 0.0316. This findings are matching with the flow structure discussed above. The obstacles block the air flow and force it to have more contact with absorber plate. Not only forcing the air to the absorber plate, obstacles also causing more backflow. More obstacles produce higher efficiency and higher friction factor. SAH requires high efficiency or high outlet air temperature, but low friction or pressure drop. Increasing friction factor means increasing pumping power required in SAH.

Besides efficiency, Nusselt number is interesting to be analyzed. It could be calculated using Eq. (11).

$$h = \frac{Nu_D k}{D_h} \tag{11}$$

While the convection heat transfer rate and log-mean temperature difference could be calculated using Eqs. (12) and (13).

$$q = hA\Delta T_{lm} \tag{12}$$

$$\Delta T_{lm} = \frac{(T_{abs} - T_o) - (T_{abs} - T_i)}{ln\frac{(T_{abs} - T_o)}{(T_{abs} - T_i)}} \tag{13}$$

The ratio S/H of obstacles effect the Nusselt number of air flow as shown in Fig. 10. Nusselt number of air flow with obstacles are much higher than without obstacle. The highest Nu number and friction factor are 94.2 and 0.628 at ratio $S/H = 0.5$ and is only 27.2 and 0.0316 at no obstacle. Fig. 11 shows the enhancement of Nusselt number when obstacles inserted in the flow compare to air flow with no obstacle. Nusselt number enhancement was the Nusselt number with obstacles compare to Nusselt number without obstacle. When obstacles inserted with ratio $S/H = 0.5$, Nusselt number increases 3.46 times and friction factor increases 19.9 times compare to those without obstacle.

Figs. 9–11 showed the same trend of SAH's efficiency, Nusselt number, and its enhancement. From efficiency and Nusselt number perspective, point A is the best, but from friction factor perspective, point D is the best. The gradient of friction factor in segment A–B is the sharpest among other segments. While the gradient of efficiency and Nusselt number enhancement in segment A–B is the least. The efficiency and Nusselt number in point B is only slightly less than point A. The Nu enhancement in point A is 3.46 and reduce to be 3.42 in point B. Thus, the reduction is only 1.13%. While the reduction of friction factor from point A to point B is 15.1% that is from 19.9 to 16.9. Sacrifice a little efficiency or Nusselt number (convection heat transfer) but save a lot friction factor (pressure drop) shall be a wise choice. So, the optimal spacing ratio, S/H of delta-shaped obstacles attached to a v-corrugated SAH is one. Since the thermal efficiency, Nusselt number, and friction factor are non-dimensional parameters, the result

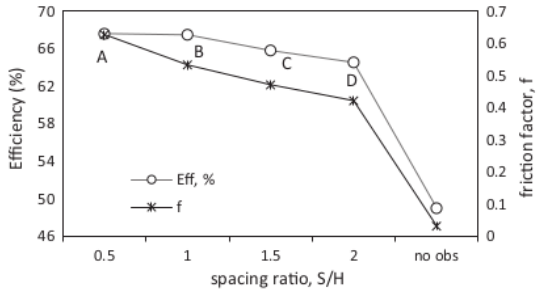

Fig. 9. The efficiency of SAH and friction factor of flow with some ratio S/H of obstacles.

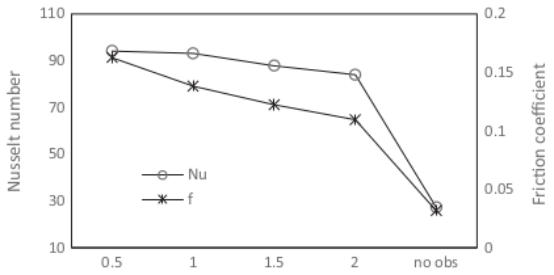

Fig. 10. Nusselt number and friction factor of air flow with obstacles inserted at some spacing ratio S/H.

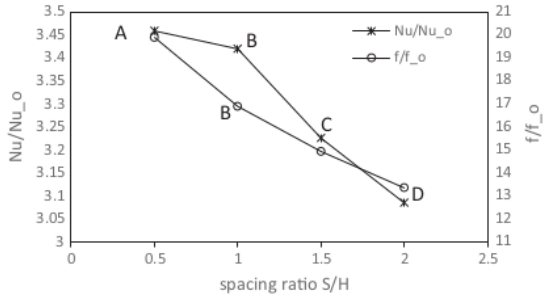

Fig. 11. Enhancement Nusselt number and increasing friction factor for some spacing ratio S/H.

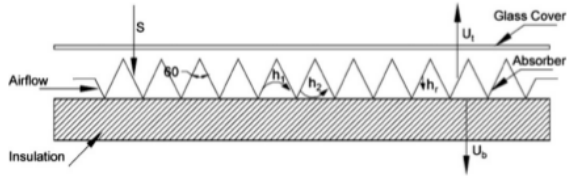

Fig. 12. A v-corrugated solar collector used by Karim & Hawlader.

could be applied to other SAH that has different geometry dimension but the same configuration.

5. Comparison to others' research

Karim dan and Hawlader (2006) worked on a flat plate solar collector with and without fin and v-corrugated absorber plate solar collector which schema is shown in Fig. 12. Dimension of the collector used is 1.8 m × 0.7 m.

The air flow rate generated by the blower in experiment of this paper that is nearest to Karim & Hawlader's SAH is 0.01164 kg/m^2 s. The comparison of the efficiency of two collectors is shown in Fig. 13.

The efficiency of SAH investigated is 0.49 and of Karim & Hawlader is 0.4, as in Fig. 13. There is a slight difference because the air flow rate is not exactly the same. Therefore, the finding in this paper is look alike with Karim & Hawlader's finding for v-corrugated absorber plate solar collector.

Akpinar dan and Koçyiğit (2010) conducted research on flat plate solar collector with two air mass flow rates, i.e. 0.0074 kg/s and 0.0052 kg/s. There were four collectors used as shown in Fig. 14. Three collectors were given obstacles on absorber flat plate. The comparison of Akpinar & Koçyiğit's collector (type II) to investigated collector is shown in Fig. 15. The efficiency of investigated collector is for air mass flow rate 0.00729 kg/s. Parameter $(T_o - T_a)/I$ of the investigated collector is slightly lower, because the air temperature across the investigated collector is lower than Akpinar & Koçyiğit collector. It is because the dimension of investigated collector is smaller than Akpinar & Koçyiğit's. The area of investigated collector was only 900 mm × 87 mm compared to Akpinar & Koçyiğit's that was 1.2 m × 0.7 m. Yet, the difference shown in Fig. 15 is not too big. It seems a good conformity between the investigated collector and Akpinar & Koçyiğit's.

Bekele et al. (2011) conducted experimental investigation on flat plate SAH with delta-shaped obstacles mounted on the absorber surface as shown in Fig. 16. Some parameter to be investigated by Bekele et al. were Reynolds number (from 3400 to 27,600), longitudinal pitch of the obstacles P_l/e (from 3/2 to 11/2), and relative obstacle height, e/H (from 0.25 to 0.75). The smaller P_l/e and the higher e/H, the efficiency is higher. The term "e" used by Bekele et al., means obstacle's height and "H" means the height of the channel. Bekele et al. used P_l/e while the investigated collector used S/H term. The "S" that indicates spacing of obstacles is the same with "P_l" that indicates longitudinal pitch (spacing). The comparison of Bekele et al.'s collector and collector being investigated (height of obstacle to channel's height, $e/H = 0.6$ and spacing or longitudinal pitch, $P_l/e = 1$ and 3/2) is shown in Fig. 17.

For smooth duct or no obstacle installed, the Nusselt number of investigated collector is higher than Bekele et al.'s. It is because the channel of investigated collector is triangular. This is consistent with the finding of Tao et al. (2007), Karim dan and Hawlader (2006),

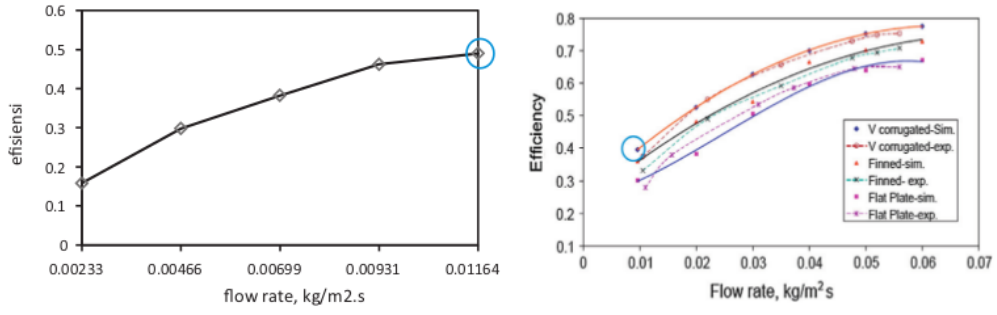

(a) Collector investigated (b) Karim & Hawlader's collector

Fig. 13. Comparison of the efficiency of collector investigated to Karim & Hawlader's.

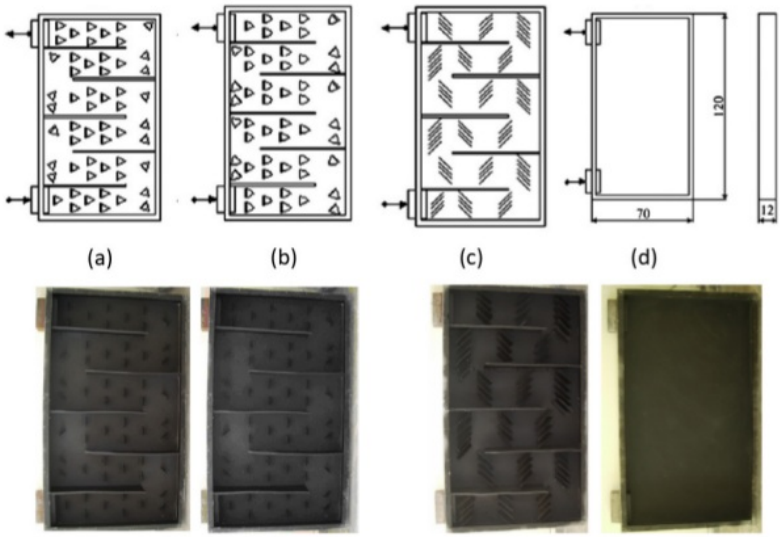

Fig. 14. Schematic views of absorber plates: (a) with triangular type obstacles, (b) with leaf type obstacles, (c) with rectangular type obstacles, and (d) without obstacles (Akpinar dan and Koçyiğit, 2010).

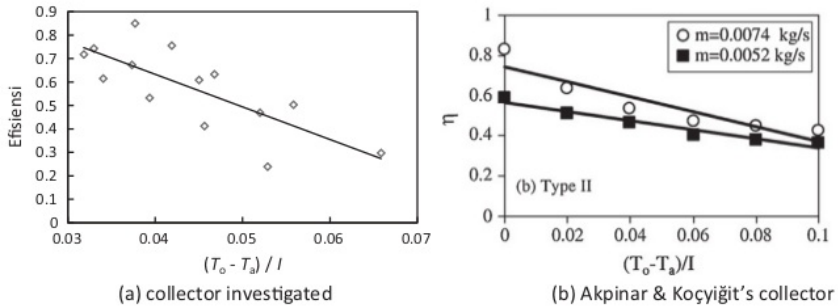

Fig. 15. Comparison of efficiency of Akpinar & Koçyiğit's collector and investigated collector.

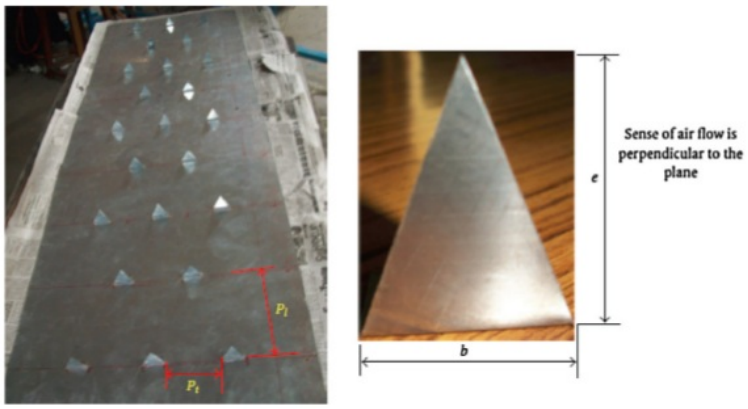

Fig. 16. Photographic view of plate with delta-shaped obstacles mounted.

Choudhury dan and Garg (1991), Naphon (2007), Islamoglu dan and Parmaksizoglu (2003). Yet, the result of Bekele et al.'s and the investigated collector show the same trend, i.e. the smaller P_1/e gives higher Nusselt number. It means more obstacles increase heat transfer to the air. The relative obstacle height used in Bekele et al.'s

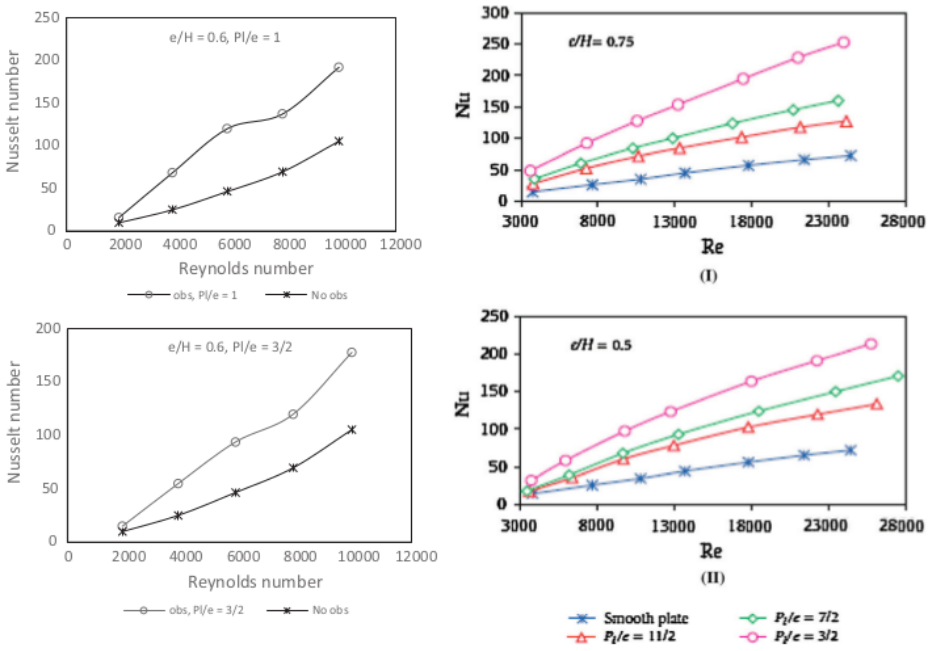

Fig. 17. Comparison of Nusselt number of Bekele et al.'s collector and investigated collector.

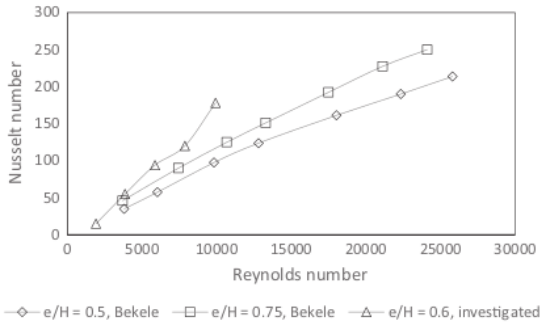

Fig. 18. Comparison of Nusselt number of Bekele et al.'s and investigated collector for $P_l/e = 3/2$.

collector was 0.5 and 0.75, while in the investigated collector was 0.6. The comparison of the results is shown in Fig. 18. When Reynolds number around 10,000 and ratio $P_l/e = 3/2$, Nusselt number of investigated collector was 178 for $e/H = 0.6$ and Nusselt number of Bekele et al. was 98 for $e/H = 0.5$ and 125 for $e/H = 0.75$. Like in collector without obstacle, the Nusselt number of investigated collector is also slightly higher than from Bekele et al. Yet, the result from this investigated collector is showing the same trend with the finding of Bekele et al.

6. Conclusion

From numerical studies in a v-corrugated duct, it is found that backflow between obstacles and high velocity in the gap between obstacles and absorber plate causes the flow became more turbulent and enhanced the convection heat transfer between the air and the absorber plate. Thus, when it is applied to SAH, it will improve its efficiency but increase the air pressure drop.

Obstacles placed in a small spacing will increase Nusselt number (convection heat transfer) and friction factor (pressure drop). The Nusselt number enhanced from 27.2 when no obstacle used to 94.2 when obstacles inserted with $S/H = 0.5$. The Nusselt enhanced 3.46 times. The friction factor will increase from 0.0316 at no obstacle to 0.628 at ratio $S/H = 0.5$. The friction factor increased 19.9 times.

Efficiency, Nusselt number, and friction factor are decreasing as ratio S/H is increasing. When ratio S/H used is 1 instead of 0.5, Nusselt number enhancement decreased only 1.13%, but friction factor decreased 15.1%. So, sacrificing a small amount of Nusselt number but reducing a significant friction factor is advantageous. The optimal spacing ratio S/H of delta-shaped obstacles inserted in a v-corrugated SAH is one. In other words, the optimal spacing of obstacle equals to its height.

Acknowledgements

Here, I am very grateful for the support from Kopertis Wilayah VII Jawa Timur, Kementerian Pendidikan dan Kebudayaan by providing Research Grant under contract No: 0004/SP2H/PP/K7/KL/II/2012.

References

Tao, L., Wen, X.L., Wen dan, F.G., Chan, X.L., 2007. A Parametric study on the termal performance of a solar air collector with a V-groove absorber. Int. J. Green Energy 4, 601–622.

Karim dan, M.A., Hawlader, M.N.A., 2006. Performance investigation of flat plate, V-corrugated and finned air collector. Energy 31, 452–470.

Choudhury dan, C., Garg, H.P., 1991. Design analiysis of corrugated and flat plate solar air heaters. Renew. Energy I (5/6), 595–607.

Naphon, P., 2007. Heat transfer characteristics and pressure drop in channel with V corrugated upper and lower plates. Energy Convers. Manage. 48, 1516–1524.

Islamoglu dan, Y., Parmaksizoglu, C., 2003. The effect of channel height on the enhanced heat transfer characteristics in a corrugated heat exchanger channel. Appl. Therm. Eng. 23, 979–987.

Promvonge, P., 2010. Heat transfer and pressure drop in a channel with multiple 60° V-baffles. Int. Commun. Heat Mass Transfer 37, 835–840.

Kurtbas dan, I., Turgut, E., 2006. Experimental investigation of solar air heater with free and fixed fins: efficiency and exergy loss. Int. J. Sci. Technol. 1 (1), 75–82.

Romdhane, B.S., 2007. The air solar collectors: comparative study, introduction of baffles to favor the heat transfer. Sol. Energy 81, 139–149.

Ho, C.-D., Yeh dan, H.-M., Chen, T.-C., 2011. Collector efficiency of upward-type double-pass solar air heaters with fins attached. Int. Commun. Heat Mass Transfer 38, 49–56.

Abene, A., Dubois, V., Le Ray dan, M., Oagued, A., 2004. Study of a solar air flat plate collector: use of obstacle and application for the drying of grape. J. Food Eng. 65, 15–22.

Esen, H., 2008. Experimental energy and exergy analysis of a double-flow solar air heater having different obstacles on absorber plates. Build. Environ. 43, 1046–1054.

Ozgen, F., Esen dan, M., Esen, H., 2009. Experimental investigation of thermal performance of a double-flow solar air heater having aluminium cans. Renew. Energy 34, 2391–2398.

Akpinar dan, E.K., Koçyiğit, F., 2010. Experimental investigation of thermal performance of solar air heater having different obstacles on absorber plates. Int. Commun. Heat Mass Transfer 37, 416–421.

Bekele, A., Mishra dan, M., Dutta, S., 2011. Effects of delta-shaped obstacles on the thermal performance of solar air heater. Hindawi Publishing Corporation: Advances in Mechanical Engineering 2011, 10 pages.

Esen, H., Ozgen, F., Esen dan, M., Sengur, A., 2009a. Modelling of a new solar air heater through least-squares support vector machines. Expert Syst. Appl. 36, 10673–10682.

Esen, H., Ozgen, F., Esen dan, M., Sengur, A., 2009b. Artificial neural network and wavelet neural network approaches for modelling of a solar air heater. Expert Syst. Appl. 36, 11240–11248.

Handoyo, E.A., Ichsani, D., Sutardi, Prabowo dan, 2014. Experimental studies on a solar air heater having V-corrugated. Appl. Mech. Mater. 493, 86–92.

Incropera dan, F.P., DeWitt, D.P., 2002. Fundamentals of Heat and Mass Transfer, fifth ed. John Wiley & Sons, s.l..

ASHRAE, 1986. Method of Testing to Determine the Thermal Performance of Solar Collectors. ASHRAE, Atlanta.

I. FLUENT, Fluent User's Guide, 2003.

Zhangdan, L., Liu, Z., 2009. A numerical simulation of the flow in a diffusing S-duct inlet. Mod. Appl. Sci. 3 (4), 111–116.

Kirkgoz, M.S., Onerdan, A.A., Akoz, M.S., 2009. Numerical modeling of interaction of a current with a circular cylinder near a rigid bed. Adv. Eng. Softw. 40, 1191–1199.

Duffie dan, J.A., Beckman, W.A., 1991. Solar Engineering of Thermal Processes, second ed. John Wiley & Sons Inc, penyunt.

Numerical Studies on the Effect of Delta-Shaped Obstacles

ORIGINALITY REPORT

16%	16%	16%	7%
SIMILARITY INDEX	INTERNET SOURCES	PUBLICATIONS	STUDENT PAPERS

PRIMARY SOURCES

1	fr.scribd.com Internet Source	4%
2	aip.scitation.org Internet Source	3%
3	jacm.scu.ac.ir Internet Source	2%
4	Azim Doğuş Tuncer, Ataollah Khanlari, Adnan Sözen, Emine Yağız Gürbüz, Ceylin Şirin, Afsin Gungor. "Energy-exergy and enviro-economic survey of solar air heaters with various air channel modifications", Renewable Energy, 2020 Publication	1%
5	Raj Kumar, Ranchan Chauhan, Muneesh Sethi, Anil Kumar. "Experimental study and correlation development for Nusselt number and friction factor for discretized broken V-pattern baffle solar air channel", Experimental Thermal and Fluid Science, 2017 Publication	1%

6	www.scientific.net Internet Source	1%
7	link.springer.com Internet Source	1%
8	www.dccc.iisc.ernet.in Internet Source	1%
9	Submitted to iGroup Student Paper	1%
10	Younes Menni, Ahmed Azzi, A. Chamkha. "Modeling and analysis of solar air channels with attachments of different shapes", International Journal of Numerical Methods for Heat & Fluid Flow, 2019 Publication	1%
11	www.oalib.com Internet Source	1%

Exclude quotes	On	Exclude matches	< 1%
Exclude bibliography	On		